IOP Publishing Smart Materials and Structures
Smart Mater. Struct. **24** (2015) 035008 (10pp) doi:10.1088/0964-1726/24/3/035008

Design and experimental characterization of a NiTi-based, high-frequency, centripetal peristaltic actuator

E Borlandelli[1], D Scarselli[1], A Nespoli[2], D Rigamonti[2], P Bettini[1], M Morandini[1], E Villa[2], G Sala[1] and M Quadrio[1]

[1] Politecnico di Milano, Dipartimento di Scienze e Tecnologie Aerospaziali, Via La Masa 34, I-20156 Milan, Italy
[2] CNR IENI, Unità di Lecco, C.so Promessi Sposi 29, I-23900 Lecco, Italy

E-mail: elena.borlandelli@polimi.it

Received 18 September 2014, revised 17 December 2014
Accepted for publication 19 December 2014
Published 3 February 2015

Abstract

Development and experimental testing of a peristaltic device actuated by a single shape-memory NiTi wire are described. The actuator is designed to radially shrink a compliant silicone pipe, and must work on a sustained basis at an actuation frequency that is higher than those typical of NiTi actuators. Four rigid, aluminum-made circular sectors are sitting along the pipe circumference and provide the required NiTi wire housing. The aluminum assembly acts as geometrical amplifier of the wire contraction and as heat sink required to dissipate the thermal energy of the wire during the cooling phase. We present and discuss the full experimental investigation of the actuator performance, measured in terms of its ability to reduce the pipe diameter, at a sustained frequency of 1.5 Hz. Moreover, we investigate how the diameter contraction is affected by various design parameters as well as actuation frequencies up to 4 Hz. We manage to make the NiTi wire work at 3% in strain, cyclically providing the designed pipe wall displacement. The actuator performance is found to decay approximately linearly with actuation frequencies up to 4 Hz. Also, the interface between the wire and the aluminum parts is found to be essential in defining the functional performance of the actuator.

Keywords: shape memory alloy, actuator, high frequency, cooling, peristalsis, centripetal

(Some figures may appear in colour only in the online journal)

1. Introduction

The energy expenditure related to transportation (of people and goods, via ground, air or water) is a subject area that is rightfully attracting much attention from the world-wide research community. Whenever a solid body has a relative motion with a fluid (be it air or water), a frictional drag due to the fluid viscosity arises, and this implies an energetic cost. When the flow motion takes place in the turbulent regime as opposed to the laminar one, this energetic cost is much higher: the additional energy is not used for useful work but simply wasted to increase the internal energy of the fluid, i.e. to increase its temperature. In many applications, the flow motion is turbulent, hence a large research effort is currently devoted to developing techniques to decrease skin-friction drag down to the laminar level [1].

A wide range of strategies and actuators are under active development; from simple modifications of the wall geometry [2] to medium-complexity open-loop forcing strategies [3] to more sophisticated controls where sensors and actuators are placed on the wall of the body and used to implement a feedback control law [4]; from miniaturized MEMS-based sensors and actuators [5] to brand-new actuation concepts, like DBD-plasma [6], synthetic jets [7], etc.

Very recently, an innovative technique has been proposed by Fukagata's group in Tokyo [8] that applies to duct flows. It consists in varying in time the geometry of the duct, by creating sinusoidal waves of wall-normal deformation

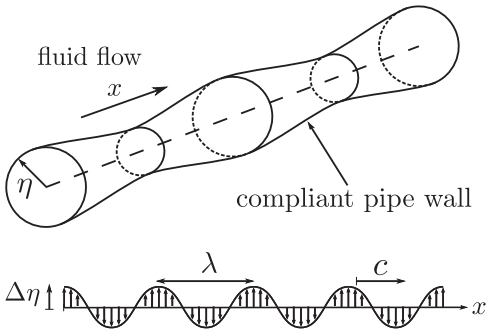

Figure 1. Sketch illustrating the geometry of a pipe flow with peristaltic waves. The fluid flow is toward the positive x direction. The deformation (peristaltic) wave travels along the x axis in a plane or circular duct delimited by deformable walls, and is characterized by maximum peak-to-peak displacement $2\eta_{max}$, wavelength λ and phase speed c. Each wall point experiences a displacement $\Delta\eta(x, t) = \eta_{max} \sin(2\pi/\lambda(x - ct))$.

traveling in the streamwise direction. We name this technique the peristaltic traveling waves. A sketch of the flow geometry and of the forcing is given in figure 1.

Numerical simulations in an idealized setup suggested [8] that a turbulent wall flow could be transformed into fully laminar by this type of forcing. In our lab a facility is already available where an entirely different technique for the reduction of turbulent drag [9] has been recently tested [10]. This facility is a convenient rig where the concept of peristaltic wave can be experimentally demonstrated. In our actuators, the peristaltic deformation will be obtained by placing several shape memory alloy (SMA) devices along the external surface of a compliant pipe.

Several studies of SMA actuators in applications involving a peristaltic deformation, for instance miniaturized fluid pumps, can be found in the literature. Solutions to generate a flow rate exist in which a SMA element is placed directly on the pipe surface. For example, a Ni–Ti wire wounded as a coil around a 5 mm diameter silicone pipe has been used as an actuator to reduce the area of the duct thus generating a displacement of fluid [11, 12]. Sassa *et al* [13] used two serial SMA sheets to build a micro pump capable of moving fluid in a 1.3 mm diameter PDMS pipe. They imposed the peristaltic deformation by inserting the tube through openings in the SMA sheet. In these works, the deformation is achieved by the Ni–Ti element directly shrinking the pipe. In other devices, peristaltic pumping is obtained by deforming a flexible tube with a structure actuated by a SMA component. A single Ni–Ti wire has been used to provide the force necessary to a plunger arm which longitudinally compresses a pipe and generates flow [14]. Guo *et al* [15] designed and tested a three-staged, four latex tubes pump. Peristalsis is obtained by alternatively compressing at the same time a couple of pipes, with extrusion poles actuated by two couples of antagonistic SMA springs. Another application of peristaltic deformation is generation of locomotion in worm-like robot devices [16, 17], where a mesh-tubed structure is equipped by SMA springs wrapped over its surface in a spiral pattern. The locomotion is realized by controlling the wire deformation with peristaltic waves.

In the cited works, peristaltic deformation of a tube-like structure is used to generate a fluid motion or a worm-like motion. This contrasts with our aim of using SMA-based actuators to generate a traveling wave along the compliant wall of a pipe and to obtain a reduction of the turbulent skin-friction drag. As locomotion or fluid pumping are not our goals, a new type of actuator must be designed, which is intended to centripetally shrink the diameter of the pipe by a limited and well controlled extension, and to act at a prescribed frequency. Such actuators will be placed along the duct, and their synchronized action should generate the desired peristaltic waves. As a first step towards the design of the whole actuation system, the present paper describes the design, optimization and experimental characterization of a single actuator. Particular care is devoted to optimize the functional properties of SMA wire, as the physics of near-wall turbulent flows dictates severe requirements for the actuators, that must cyclically achieve large deformations at large actuation frequency on a sustained basis.

2. Actuating SMAs at high frequency

The near equiatomic NiTi system is the most recognized SMA, owing to its excellent mechanical properties related to the high strain recovery (shape memory effect), as well as the high pseudoelastic and damping behavior. In particular, the shape recovery is typically exploited in the actuator field, where the material performs against an external load inducing mechanical work [18–20]. At the base of these mechanical attitudes, there is a thermoelastic martensitic transformation between two solid phases, austenite (BCC lattice) and martensite (monoclinic lattice), that are stable in two critical temperature ranges. These intervals are delimited by conventional values that indicate the onset and offset of the direct transition from austenite to martensite during cooling (martensite start M_s and finish M_f), and of the reverse transformation during which austenite is created from martensite (austenite start A_s and finish A_f). The forward and reverse transformations between the two phases shows a thermal hysteresis usually ranging from 20 to 40 °C [21].

The macroscopic shape recovery under load of a single NiTi element during a thermal cycle is largely studied and it is well employed in the actuation field. In this application, a long fatigue life is achieved when the NiTi material works under a typical stress varying from 150 to 200 MPa. In this working condition, the NiTi material is able to recover up to 4% of deformation [22] during each heating/cooling cycle in tensile configuration. The Joule effect usually allows for a relatively fast heating of the NiTi component [23]; the cooling process, however, is more critical for high-frequency applications, and requires more time, owing to the material diffusivity properties as well as heat exchange phenomena which may interfere with the dynamic response of the actuator. Normally, cooling is achieved by natural convection and,

therefore, the actuator dimensions play an important part in the duration of one single thermo-mechanical loop.

In the past, several studies have attempted to improve the dynamic response of NiTi actuators, although many target one-shot actuation only. A large portion of these works employs forced cooling. The most obvious strategy is fluid cooling, achievable with different heat transfer medium (air, water, oil) and velocity (low or high speed, jet). Other ways to remove heat from the SMA element can be the contact with a heat sink, Peltier modules or silicone grease.

According to Tadesse *et al* [24], who compared various active cooling techniques with natural convective cooling in ambient air, low-speed forced air cooling has a small effect on the response time, reducing it by 35%, whereas heat sinking and high-speed forced air reach a 75% reduction, while fluid quenching a 87% one. The use of thermal gel is ineffective because the dissipation overcomes the Joule heating of the wire and the viscosity blocks its contraction. Bergamasco *et al* [25] used a water system to improve the cooling response of a SMA robotic actuator. Their device consisted of two antagonist SMA springs made of a 0.5 mm NiTi wire, working in a box under a continuous flow of distilled water. The resulting frequency cut-off of such actuator equipment is between 1 and 2 Hz. Howe *et al* [26] improved the actuation response of a 0.075 mm NiTi wire by using a feed-forward analytical compensation during heating and a pneumatic system during cooling, reaching a final frequency response between 6 and 7 Hz. This good result is probably due to the small dimension of the NiTi sample. Hashimoto *et al* [27] showed that the best cooling performances are achieved with an aluminum heat sink. More precisely, they demonstrated that a wire encapsulated in a circular shaped aluminum heat sink (thus providing the maximum contact surface) has a cooling rate faster than fluid quenching methods. In their work they also used Si rubber sheet and Si grease to isolate electrically the heat sink when the NiTi wire is heated with current.

If active also during the heating phase, these cooling methods have the drawback of increasing the power consumption needed to activate the element. If the SMA actuator is dissipating while being heated, the transformation will not occur until enough energy is generated to overcome the dissipation. Because the common heating system is the Joule effect, this implies a remarkable increase in the electrical power required. A possible solution is the use of a mobile heat sink that comes off the SMA during heating, reducing the power amount compared to an equivalent fixed heat sink [28]. Luchetti *et al* [29] reduced the thermal hysteresis by using a silicone cover to uniform the conductivity coefficient on the heat exchanging surface. In the case of jet fluid cooling, very rapid heat transfer occurs between the jet fluid and the SMA actuator. Zhang *et al* proposed to both cool and heat the SMA element with a liquid jet, obtaining quite good shape deformation performance of the actuator [30]. Finally, because the martensitic transformation has a thermoelastic behavior, the cooling evaluation is complicated by the need to consider not only the parameters of the thermal exchange (heat transfer parameter, dimensions of the SMA element, etc), but also the mechanical parameters such as load and strain. It should be considered, for example, that cooling time decreases with increasing load, as the transformation temperatures rise with increasing load and activation is consequently reached at higher temperature. The cooling gap remains the same, but the exchange occurs at a higher temperature and so is more efficient [24]. Similarly the transformation temperature increases also with a larger value of operational strain obtaining the same effect [25].

Other approaches are based on control methods that improve the time response of SMA by directly acting on the heating rate. Teh and Featherstone [31] presented a control scheme of antagonist SMA wires, achieving a frequency operation of 2 Hz with 0.1 mm diameter SMA wires. In their work, they used the electrical resistance signal as an indicator of temperature to avoid overheating and let the SMA wires work at a temperature always lower than A_f. An analogous study was reported by Nakshatharan *et al* [32], where strain is used as temperature controller of 0.15 mm antagonistic NiTi wires. In this work, temperature is indirectly maintained between M_s and A_f temperature limits by partial transformation strain; in this way, a working frequency of 1 Hz is achieved.

Finally, we have examples of works in which the operation frequency is improved thanks to the very small dimension of the NiTi wires [27]. However, this strategy poses a strict limit on the maximum reachable wire actuation force.

3. Design of the actuator

Our goal is to design and experimentally characterize a SMA-actuated device to carry out cyclic radial deformation of a compliant pipe. The design has both geometrical and temporal requirements: the device must shrink the pipe radius while preserving the circular shape of its section; must achieve a minimum amount of linear deformation (8%); must work continuously at a given actuation frequency.

3.1. Performance requirements

The basic principle behind the actuation device is to convert the linear contraction of a heated SMA wire into a radial displacement, as sketched in figure 2(s).

As previously stated, a NiTi element which works cyclically in tensile configuration under a typical stress can recover up to 4% of deformation, providing a constant, stable and reliable contraction regardless of the number of cycles. Our application has never been experimentally investigated, but on the basis of the two available numerical studies [8, 33] it can be estimated that the best-performing peristaltic waves are achieved with a pipe contraction of 8%, which is our design target. In order to reach that contraction by using a NiTi wire working at a percentage lower than 4%, we need to design a rigid device that is able to geometrically amplify the wire linear contraction, as illustrated in figure 2(b). For a device height h and a desired shrinking ratio

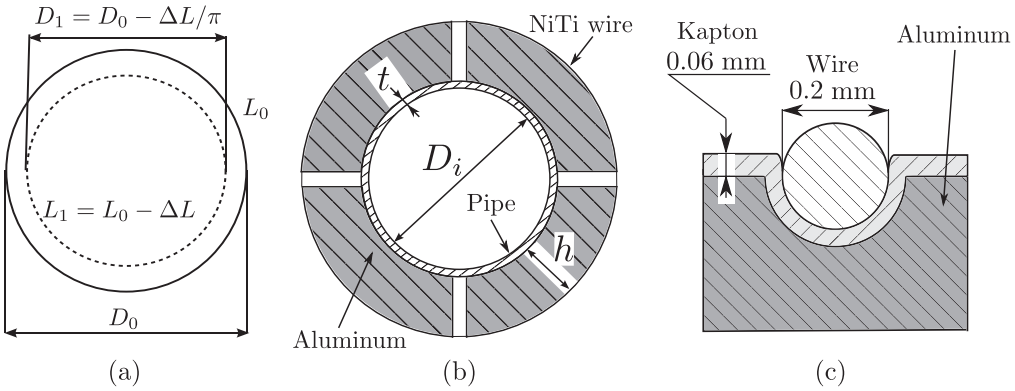

Figure 2. (a) A variation ΔL of the length of the circumference L_0 results in a variation $\Delta L/\pi$ of the diameter D_0. (b) Section of pipe and actuator, showing the device supporting the SMA wire. The pipe has internal diameter D_i and thickness t. The wire support has height h, so that the NiTi wire length is $\pi(D_i + 2t + 2h)$. (c) Cross-section of the grooved interface between the SMA wire and the actuator. A thin Kapton layer (60 μm) is placed between aluminum and wire to provide electrical insulation. Groove diameter is chosen to maximize the contact surface between Kapton and the wire.

$\alpha = (D_1 - D_0)/D_0$ the contraction of the wire β is

$$\beta = \frac{L_1 - L_0}{L_0} = \frac{\alpha}{\frac{2h}{D_0} + 1}, \tag{1}$$

and can be tuned between $\beta = \alpha$ for $h = 0$ and $\beta \to 0$ for $h \to \infty$.

A rigid frame is also useful to guide the wire around the pipe, to hold it in position, to properly link it to the electrical contacts and to ensure that the pipe section remains almost circular during the actuation. As shown in figure 2(b), the actuator is made by four circular sectors, with an internal diameter that fits the external pipe diameter, that can slide over the pipe wall. Each of the four actuator parts has a groove running along the external surface that keeps the wire in position during the actuation, so that the contraction occurs always in the same cylinder directrix. Besides, a wire-clamping system is located in one of the four parts of the actuator.

The displacement resulting from the contraction of the SMA wire has to be transferred through the solid aluminum parts and pipe wall to the fluid inside the pipe. To this end, it is necessary to select a flexible pipe made by a material which is compliant enough to deform without distorting the circular shape and without requiring significant stress. We choose a silicone pipe (50 shore A) with internal diameter $D_i = 40$ mm and thickness $t = 3$ mm. Once the pipe dimensions are known, we set the wire contraction factor $\beta = 3\%$ to ensure durability, and the shrinking ratio $\alpha = 8\%$. Then formula (1) can be used to obtain a height of the device $h = 30$ mm.

During every actuation cycle, a contraction of the wire takes place during heating, while during the cooling phase, the SMA wire is reset to its initial length. The recovery force required for re-arming is often obtained via calibrated weights or an antagonistic wire. In the present case, because of the specific application, we exploit both the fluid pressure inside the pipe, that greatly contributes to the re-arm force, and (to a lesser degree) the elastic reaction of the elastomer.

Once the device geometry has been figured out, the thinnest wire which provides the necessary actuation force is selected, as it should be best at meeting the fast cooling requirements. To estimate the stress σ acting in the wire we assume a simplified model in which the silicone stiffness is negligible. This assumption leads to the formula

$$\sigma = \frac{pD_i z}{\pi D_w^2/2}, \tag{2}$$

where D_w is the wire diameter, p is the internal pressure and z is the width of the device out of its plane. The following set of parameters

$$z = 8 \text{ mm}, \qquad p = 0.4 \text{ bar}, \qquad D_w = 0.2 \text{ mm}$$

results in $\sigma \approx 200$ MPa, which is the optimal working stress for the considered wire, as discussed in the introduction.

Among the cooling methods presented in the introduction, the most performing strategies are forced convection in liquid environment, e.g. water and oil, and heat sinking. Experimental evidence [27] suggests that the latter can perform as well as the former, if a good interface between the wire and the heat sink is provided. Therefore, to avoid an unpractical immersion of a long pressurized pipe in a liquid bath, we decided to pursue a heat sink method associated to a forced airflow. The actuator itself is used to soak and dissipate thermal energy, hence the device must be made of a highly conductive material, and the interface between the wire and the heat sink surface must be as large as possible. To this end, the actuator is made by aluminum (thermal conductivity $k = 200 \text{ W m}^{-1} \text{ K}^{-1}$) and the wire is seated within a semi-circular shaped groove that fits the wire diameter. To ensure electrical insulation a thin adhesive Kapton layer (60 μm, $k = 0.12 \text{ W m}^{-1} \text{ K}^{-1}$) is put between the aluminum surface and the wire, see figure 2(c).

3.2. SMA choice and characterization

Applications involving SMA as actuators must take into account a material with stabilized properties over a typical

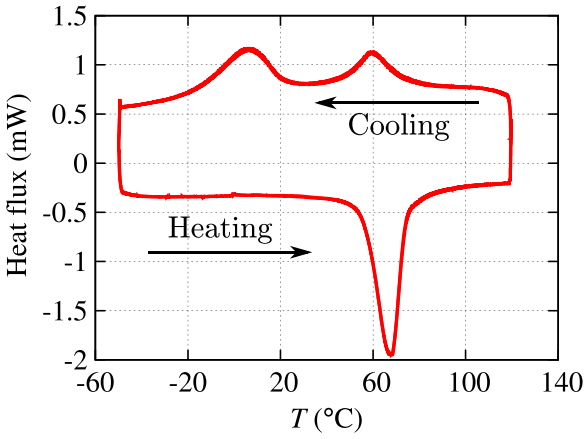

Figure 3. DSC curve of the 0.2 mm wire.

lifetime. In our application, the SMA should ensure repeatability in terms of stress and strain for approximately 10^5 cycles. Recently, manufacturers of NiTi material have been developing different types of NiTi products suitable for actuator applications. We work with a Smartflex wire of 0.2 mm in diameter developed by SAES Getters; according to the manufacturer, the wire has a maximum stroke of 5.5% and it is stabilized to work at 150 MPa at 3.5% stroke for a number of cycles larger than 2×10^5.

To characterize the thermo-mechanical properties of the chosen Smartflex wire we experimentally evaluate the phase transformation temperatures through DSC, stress–strain (at constant temperature) and strain–temperature (at constant stress) curves.

Figure 3 shows the DSC curve of the as received SMA wire. In the cooling ramp, the two main peaks are associated to two distinct martensitic transformations: the first is related to B2–R and the second to R–B19 transitions, where B2, R, and B19 stand for the cubic (austenite), the rhombohedral, and the monoclinic structures (martensite), respectively. The single peak visible in the heating ramp is related to the direct B19–B2 transition. According to DSC results, we find that A_f temperature is 75 °C and the wire is in martensite phase at room temperature.

The plot in figure 4(a) shows curves in the strain–temperature plane at constant stress. We note that the curve for 300 MPa is not closed, implying a residual deformation (0.2%) due to wire yielding. Moreover, we use these curves to evaluate the Clausius–Clapeyron constant for our wire, which results 8.72 MPa/°C. Finally, figure 4(b) shows how stress and strain are related to each other at various temperatures.

4. Tests and results

4.1. Setup

The setup for the actuator characterization is sketched in figure 5(a); a photograph of the experimental apparatus is depicted in figure 5(b). A short segment (200 mm) of silicone pipe is sustained by a metal fixture and inflated by a pressure-controlled external line. The pipe is sealed at its extremities by two stop valves, granting access for an endoscopic probe. The actuator system, composed by the NiTi wire and the Al support and heat sink, is clamped directly on the pipe and it is controlled by a power MOSFET switch driven by a signal generator and a dc power supply. This allows us to cyclically heat the wire according to a desired wave form. In this study, to tune the heating and cooling time of the NiTi wire we always use a square wave. Figure 6(a) defines the tension waveform applied to the MOSFET gate. Since we are interested in evaluating the performance of our device for a continuous and cyclic actuation, we set up an experiment to deduce peak-to-peak displacement from the temporal trace of peristaltic displacement. Both the radial external displacement of the device and the internal wall deformation due to the peristaltic movement are independently measured. An external laser measuring system is employed to obtain the time history of the wall deformation at a sampling rate of 500 Hz, as sketched in figure 6(b). Simultaneously, we use an endoscopic camera synchronized with the actuation signal by means of an external triggering device. The camera shoots two pictures, respectively at the end of heating and cooling phases. The displacement is evaluated by counting the number of pixels between reference points identified by markers of known size previously placed on the internal wall, see figure 6(c). The endoscopic measurements, although available at two time instants only, allow us to validate the data acquired by the laser system.

Jointly with the motion history of the actuation, the current flowing through the wire is also measured by means of a current clamp, in order to relate the current signal to the measured displacement. A *K*-type thermocouple additionally acquires the temperature of the aluminum device, to monitor over time its effectiveness as heat sink. Finally, the temperature drift of the aluminum is mitigated by forced air convection realized with a fan.

Data acquisition is managed by a personal computer. In particular, a specific camera software controls shooting timing, triggering, settings and archives photos to hard disk. The PC also runs a LabVIEW DAQ software which acquires displacement time histories, together with the NiTi wire current measured by the current clamp.

Tests have been carried out following a fixed procedure to ensure repeatability. For each run, actuation is started with the aluminum device at room temperature (approximately 22.5 °C). Every acquisition is then carried on for a time interval of 210 s, which is twice the expected duration of the experimental run.

4.2. Results

Figure 7(a) shows a sample of the displacement history over a few cycles, in the reference configuration at a frequency of 1.5 Hz for a square wave of current 4 A, with a pipe pressure of 0.4 bar and a Kapton thickness of 60 μm. We use $t_{heating} = 0.06$ s, which corresponds to 9% duty cycle, in order to maximize the cooling time and reduce the dissipation through the heat sink during heating, since our cooling

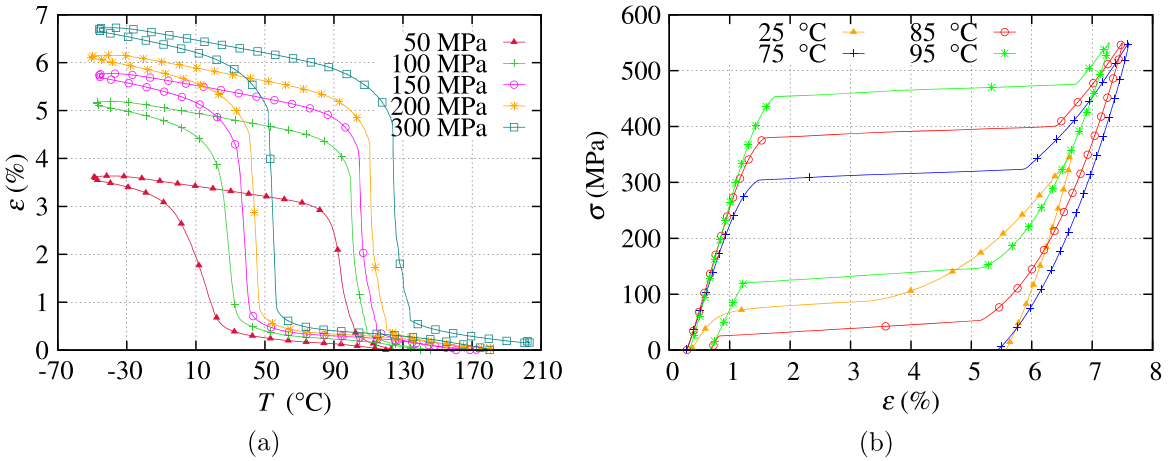

Figure 4. (a) Strain versus temperature curves and (b) stress versus strain curves for the 0.2 mm wire.

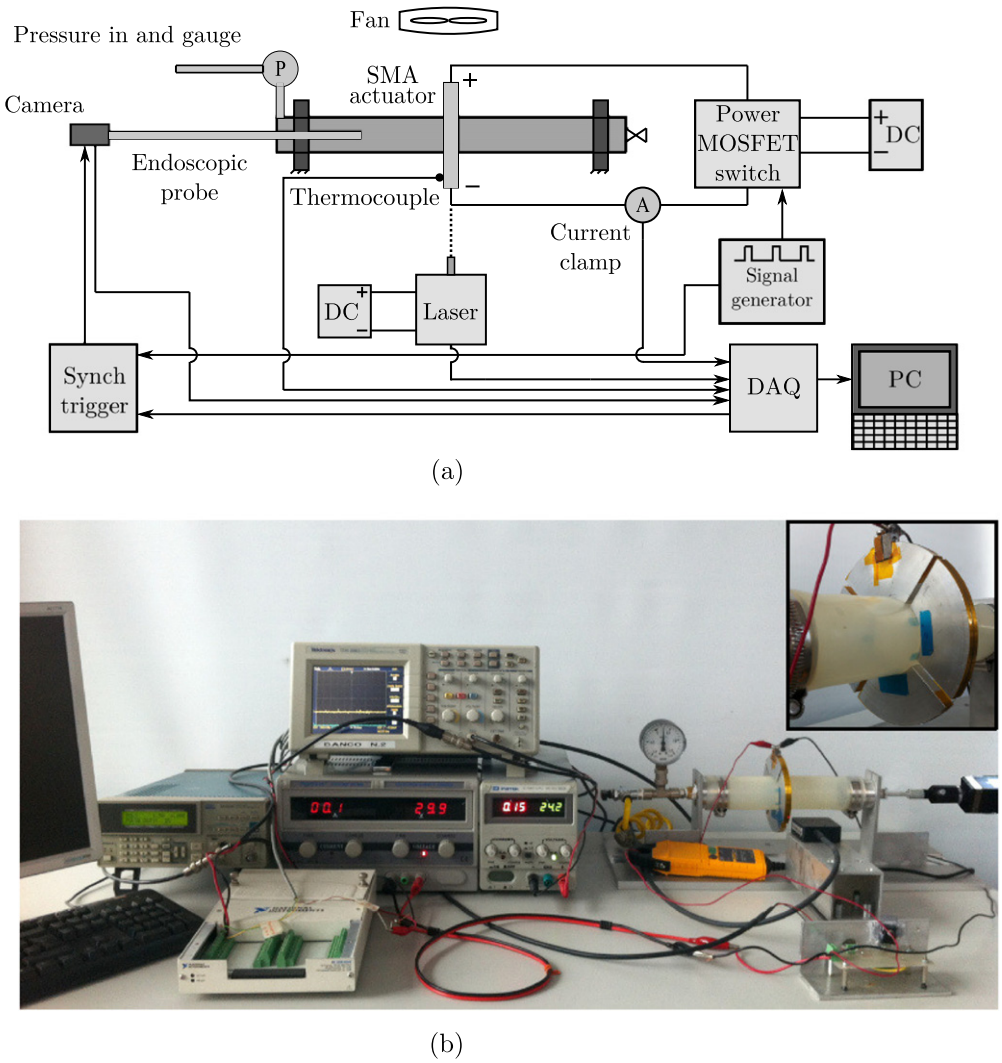

Figure 5. (a) Block diagram schematic and (b) photograph of the control and data acquisition setup, with a detailed view of the actuator (inset).

method is operating also in this phase. In this configuration, which corresponds to nearly the best performance we could achieve, a cyclic displacement $\Delta x = 1.1$ mm is obtained, with a peak value $x_{max} = 1.6$ mm, confirming the target design of the actuator. Figure 7(b) shows another sample of displacement history, with the frequency increased to 3 Hz and the other parameters unchanged. The displacement waveform nearly retains an identical shape as the one of figure 7(a), and

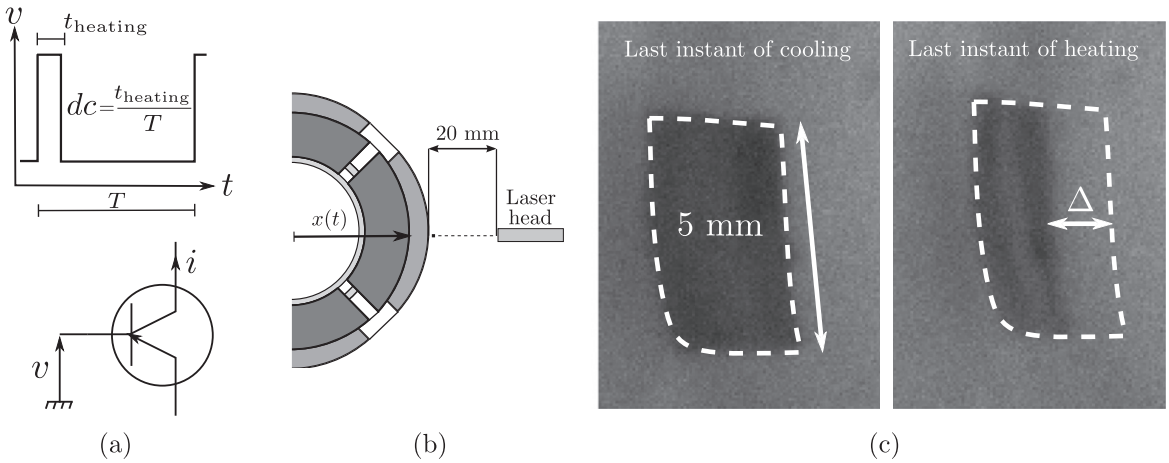

Figure 6. (a) Description of the control signal. A square wave tension v is used to pilot the gate of a MOSFET switch allowing the current i to flow through the NiTi wire. (b) Sketch of the external laser system. Sensing range is from 20 to 22 mm. Voltage output measures actual radial displacement of the actuator. (c) Example of endoscopic pictures: left and right frames depict a marker immediately before heating and cooling phase, respectively. Wall displacement is evaluated by measuring the pixel distance Δ and then converting into mm.

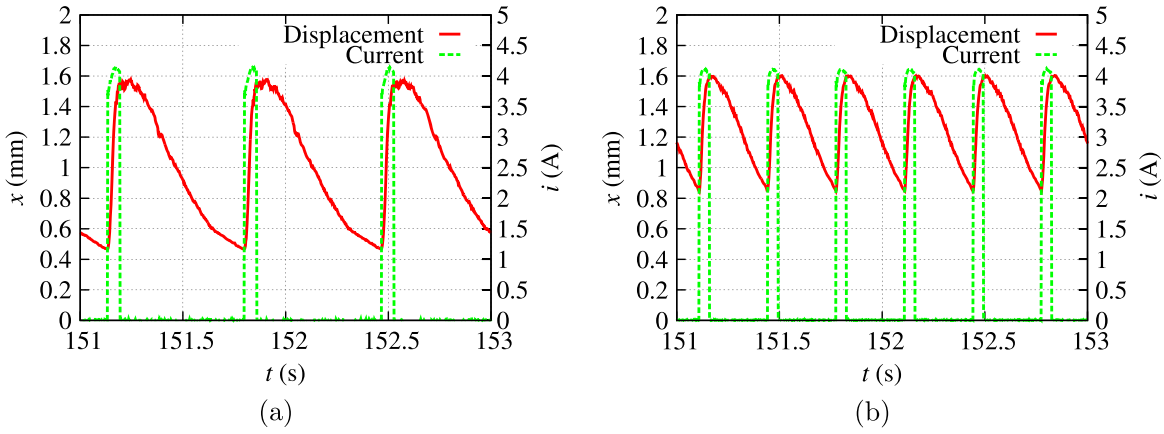

Figure 7. Displacement history for a square wave of current 4 A and $t_{heating}$ = 0.06 s. (a) Actuation frequency is 1.5 Hz. (b) Actuation frequency is 3 Hz.

also, the maximum value x_{max} remains unchanged, while the cycle amplitude Δx reduces to 0.7 mm. This effect is due to a shorter cooling time that results in lower percentage of phase transformation, thus reducing the wire recovery.

Figure 8(a) exemplifies the trend of the performance parameter Δx on varying frequency, at fixed configuration (geometry, current and $t_{heating}$). We observe that when the forcing frequency is below 0.5 Hz, a full recovery of the SMA wire is attained, i.e. peak and cyclic displacement coincide. When the actuation frequency is increased above this threshold, a progressive reduction of performance is observed, exhibiting in the decrease of Δx, while x_{max} remains constant and equal to 1.6 mm.

We also investigate the influence of the remaining parameters on the reference configuration: current duty cycle, aluminum heat sink temperature drift, electrical insulator thickness, groove radius. A test with conductive paste between the SMA wire and the groove is also described.

At the reference frequency of 1.5 Hz we test the influence of the duty cycle, i.e. $t_{heating}$, on the cycle amplitude while the energy input is kept constant, i.e. power × period = constant. Note that, to work at constant energy, power must be inversely proportional to the duty cycle. Figure 8(b) illustrates both cyclic displacement Δx and power consumption as the duty cycle changes. An increase in the duration of $t_{heating}$ is associated to reduced performance of the actuator, as the cooling phase reduces. However, short activation times, while providing better results in terms of Δx, require the same amount of energy to be pumped in the wire in a very short time, leading to large peak power consumption.

During a typical test of 210 s, the aluminum temperature exhibit a nearly linear drift, from the ambient temperature of 22.5 to 33.5 °C. During the same time, the cyclic displacement remains unchanged, as clearly shown in 8(c). Hence the aluminum frame works well as heat sink as far as its temperature is well below the temperature M_f of the wire.

If the thickness of the kapton tape is reduced from 60 to 25 μm, we notice that the cyclic displacement drops from 1.1 to 0.9 mm as shown in figure 8(d). This happens because the thinner tape implies less thermal insulation and consequently leads to a faster heat dissipation through the aluminum during the current-on phase. Higher power is consequently needed to

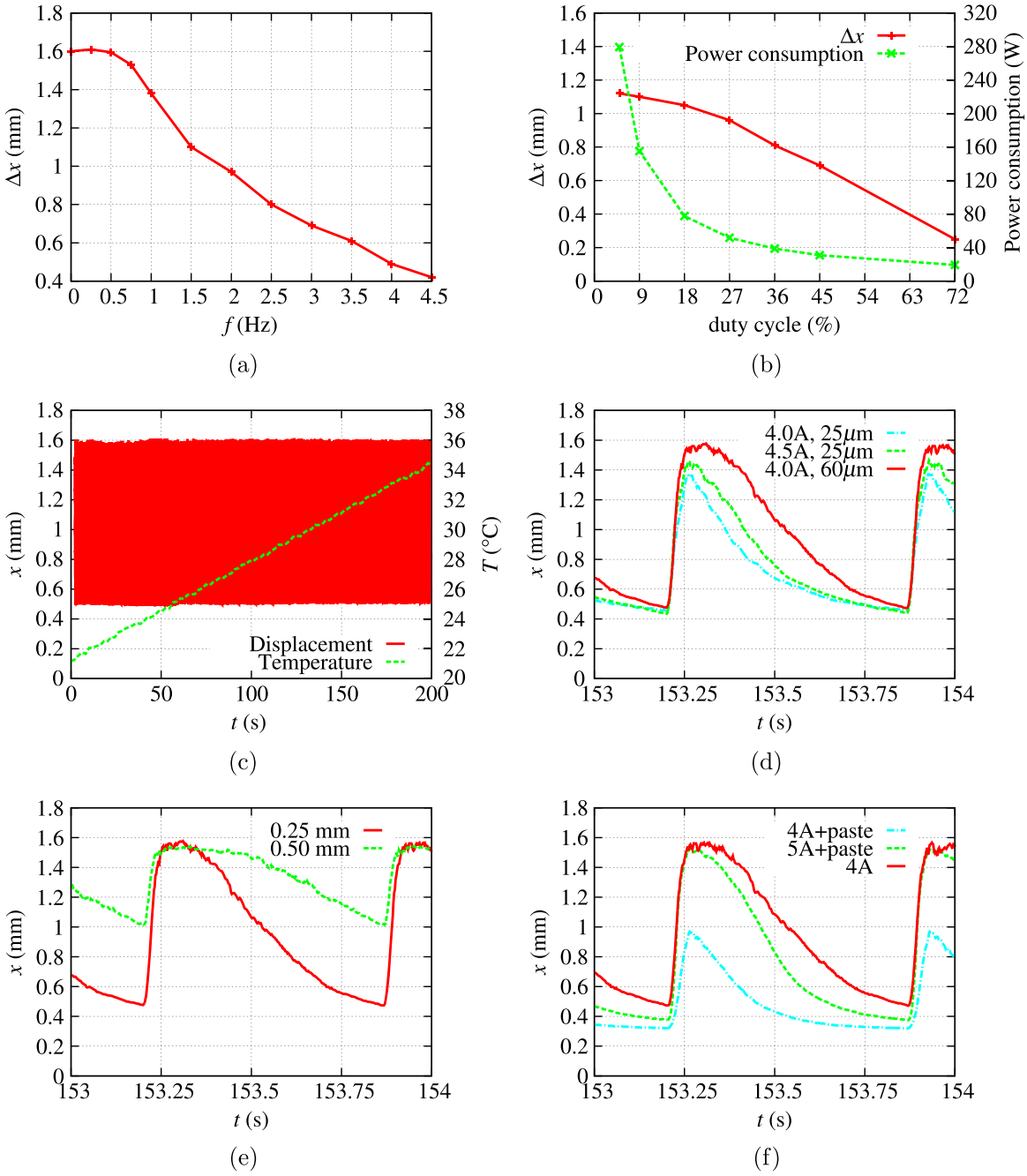

Figure 8. (a) Plot of displacement cyclic amplitude versus frequency. (b) Plot of displacement and temperature history over time for our reference configuration at a frequency of 1.5 Hz. (c) The effect of varying duty cycle while keeping constant the energy consumption for heating the wire. (d) A comparison between different Kapton tape thicknesses. (e) The influence of the groove design. (f) Effects of combining heat sink with a conductive paste.

obtain the same displacement with less kapton. Although we could increase current only from 4 to 4.5 A owing to limitation of the bench power supply, the curve at 4.5 A in figure 8(d) clearly indicates an improved displacement.

Modifications to the cross-sectional shape of the groove leads to a different mechanical and thermal coupling between the NiTi wire and the aluminum heat sink. As discussed in the Introduction, the design of the groove is the parameter that has the largest influence on the SMA performance. Figure 8(e) shows a comparison between the reference configuration with the semi-circular shaped groove that fits the wire diameter and a groove with same nominal shape but twice the diameter, hence reducing the effective contact area between wire and heat sink. While both tests show identical peak displacements, the measured displacement history is very different in cyclic values and curve slope. The deepest groove shows a slower cooling phase, due to the smaller surface area between wire and heat sink. It is also possible

that positioning the wire within a deeper groove could lead to a less efficient cooling by convection with hot air surrounding the NiTi.

Lastly, figure 8(f) investigates the benefits of combining heat sink with a conductive paste that improves the thermal coupling between wire and aluminum. The presence of the paste affects the power consumption: to achieve comparable results to the reference configuration we need to increase the current up to 5 A. The larger (negative) slope of the curve suggests a more efficient cooling phase, but the small improvement of the cyclic displacement of only 0.1 mm has to be considered in view of the increased current requirements.

5. Conclusions

In this work we have designed and characterized the key component of a peristaltic device, that employs a 0.20 mm diameter NiTi wire. The actuator must deform a compliant, 40×46 mm silicone pipe with a frequency and displacement typical of flow control applications, hence with peculiar requirements with respect to the classic peristaltic pumping. In our design, the wire is supported by a four-sectors, aluminum-made circular frame. The frame geometrically amplifies the wire contraction while naturally providing a heat sink during the cooling phase. The aluminum is electrically insulated from the wire by a 60 μm thick Kapton tape, whose thickness is crucial in determining the overall response of the system as it also acts as thermal insulation.

We tested the actuator at various frequencies, current inputs and design parameters. Statically, the actuator was capable to reduce the pipe diameter by 3.2 mm, while at the reference frequency of 1.5 Hz we were able to achieve a continuous cyclic diameter contraction of 2.2 mm. The static behavior was found to be recovered at 0.5 Hz, while we measured 0.8 mm of diameter shrinking at the highest considered frequency of 4.5 Hz. We found that the performance decay with frequency is approximately linear in the range examined. Among the design parameters considered, we discovered that the interface between the wire and the heat sink plays a fundamental role in determining the amplitude of the cyclic response of the device. Optimal performance was reached with a wire bed which maximizes the contact surface with the heat sink. Also, we found that both a thinner Kapton layer, and the use of conductive paste to amplify thermal dissipation, lead to a further improvement in the cycle amplitude Δx, at the cost of a larger power expense.

Much work remains to be done. In this study, we have focused on a reference configuration, by varying several design parameters one at the time to evaluate their impact on performance. Hence, mixed parameters configurations (Kapton thickness, signal waveform, conductive paste…) remain to be addressed to possibly further improve the power efficiency of the device. Moreover, hundredths of actuators will have to be put together, working concurrently to reproduce a full traveling wave of peristaltic deformation of the pipe wall; this will certainly pose additional interesting problems that will be addressed in future work.

Acknowledgments

The financial support from DAST-PoliMi by the grant ‘An innovative technique for turbulent skin-friction drag reduction: traveling waves of peristaltic deformation’ is gratefully acknowledged. The authors wish to dedicate the present paper to the memory of the late Prof Teodoro Merlini.

References

[1] Leschziner M, Choi H and Choi K-S 2011 Flow control approaches in aerodynamics: progress and prospects *Phil. Trans. R. Soc.* A **369** 1349–51
[2] Garcia-Mayoral R and Jiménez J 2011 Hydrodynamic stability and the breakdown of the viscous regime over riblets *J. Fluid. Mech.* **678** 317–47
[3] Quadrio M 2011 Drag reduction in turbulent boundary layers by in-plane wall motion *Phil. Trans. R. Soc.* A **369** 1428–42
[4] Kim J and Bewley T R 2007 A linear systems approach to flow control *Annu. Rev. Fluid Mech.* **39** 383–417
[5] Kasagi N, Suzuki Y and Fukagata K 2009 MEMS-based feedback control of turbulence for drag reduction *Annu. Rev. Fluid Mech.* **41** 231–51
[6] Wang J-J, Choi K-S, Feng L-H, Jukes T N and Whalley R D 2013 Recent developments in DBD plasma flow control *Prog. Aerosp. Sci.* **62** 52–78
[7] Glezer A 2011 Some aspects of aerodynamic flow control using synthetic-jet actuation *Phil. Trans. R. Soc.* A **369** 1476–95
[8] Nakanishi R, Mamori H and Fukagata K 2012 Relaminarization of turbulent channel flow using traveling wave-like wall deformation *Int. J. Heat Fluid Flow* **35** 152–9
[9] Quadrio M, Ricco P and Viotti C 2009 Streamwise-traveling waves of spanwise wall velocity for turbulent drag reduction *J. Fluid Mech.* **627** 161–78
[10] Auteri F, Baron A, Belan M, Campanardi G and Quadrio M 2010 Experimental assessment of drag reduction by traveling waves in a turbulent pipe flow *Phys. Fluids* **22** 115103
[11] Prasanth K V S S D and Sreekumar M 2012 Design of a new biomimic flow pump using sma actuators *Appl. Mech. Mater.* **110** 2903–10
[12] Sagar S N and Sreekumar M 2013 Miniaturized flexible flow pump using sma actuator *Procedia Eng.* **64** 896–906
[13] Sassa F, Al-Zain Y, Ginoza T, Miyazaki S and Suzuki H 2012 Miniaturized shape memory alloy pumps for stepping microfluidic transport *Sensors Actuators* B **165** 157–63
[14] Shkolnikov V, Ramunas J and Santiago J G 2010 A self-priming, roller-free, miniature, peristaltic pump operable with a single, reciprocating actuator *Sensors Actuators* A **160** 141–6
[15] Guo S, Sun X, Ishii K and Guo J 2008 Sma actuator-based novel type of peristaltic micropump *Int. Conf. on Information and Automation (ICIA)* (Piscataway, NJ: IEEE) pp 1620–25
[16] Boxerbaum A S, Chiel H J and Quinn R D 2010 A new theory and methods for creating peristaltic motion in a robotic platform *IEEE Int. Conf. on Robotics and Automation (ICRA)* (Piscataway, NJ: IEEE) pp 1221–27

[17] Seok S, Onal C D, Cho K-J, Wood R J, Rus D and Kim S 2013 Meshworm: a peristaltic soft robot with antagonistic nickel titanium coil actuators *IEEE/ASME Trans. Mechatronics* **18** 1485–97

[18] Mammano G S and Dragoni E 2011 Increasing stroke and output force of linear shape memory actuators by elastic compensation *Mechatronics* **21** 570–80

[19] Nespoli A, Villa E and Besseghini S 2012 Thermo-mechanical properties of snake-like niti wires and their use in miniature devices *J. Therm. Anal. Calorimetry* **109** 39–47

[20] Nespoli A, Rigamonti D, Villa E and Passaretti F 2014 Design, characterization and perspectives of shape memory alloy elements in miniature sensor proof of concept *Sensors Actuators* A **218** 142–53

[21] Otsuka K and Ren X 2005 Physical metallurgy of Ti–Ni-based shape memory alloys *Prog. Mater. Sci.* **50** 511–678

[22] Mammano G S and Dragoni E 2012 Functional fatigue of Ni–Ti shape memory wires under various loading conditions *Int. J. Fatigue* **69** 71–83

[23] Bettini P, Riva M, Sala G, Di Landro L, Airoldi A and Cucco J 2009 Carbon fiber reinforced smart laminates with embedded sma actuatorspart: I. Embedding techniques and interface analysis *J. Mater. Eng. Perform.* **18** 664–71

[24] Tadesse Y, Thayer N and Priya S 2010 Tailoring the response time of shape memory alloy wires through active cooling and pre-stress *J. Intell. Mater. Syst. Struct.* **21** 19–40

[25] Bergamasco M, Salsedo F and Dario P 1989 A linear SMA motor as direct-drive robotic actuator *Proc. IEEE Int. Conf. on Robotics and Automation* (Piscataway, NJ: IEEE) pp 618–23

[26] Howe R D, Kontarinis D A and Peine W J 1995 Shape memory alloy actuator controller design for tactile displays *Proc. 34th IEEE Conf. on Decision and Control* vol 4 (Piscataway, NJ: IEEE) pp 3540–44

[27] Hashimoto M, Takeda M, Sagawa H, Chiba I and Sato K 1985 Application of shape memory alloy to robotic actuators *J. Robot. Syst.* **2** 3–25

[28] Russell R A and Gorbet R B 1995 Improving the response of SMA actuators *Proc. IEEE Int. Conf. on Robotics and Automation* vol 3 (Piscataway, NJ: IEEE) pp 2299–2304

[29] Luchetti T, Zanella A, Biasiotto M and Saccagno A 2009 Electrically actuated antiglare rear-view mirror based on a shape memory alloy actuator *J. Mater. Eng. Perform.* **18** 717–24

[30] Zhang L-x, Hu G-x and Wang Z-g 2008 Study on liquid-jet cooling and heating of the moving SMA actuator *Int. J. Therm. Sci.* **47** 306–14

[31] Teh Y H and Featherstone R 2004 A new control system for fast motion control of SMA actuator wires *The 1st Int. Symp. on Shape Memory and Related Technologies*

[32] Nakshatharan S S, Ruth D J S and Dhanalakshmi K 2014 Dynamic stabilization and rapid motion control system driven by antagonistic shape memory alloy actuators *J. Vib. Control* 1077546313520177

[33] Mamori H, Iwamoto K and Murata A 2014 Effect of the parameters of traveling waves created by blowing and suction on the relaminarization phenomena in fully developed turbulent channel flow *Phys. Fluids* **26** 015101